Int. J. Electrochem. Sci., 13 **(2018)** 11388 – 11404, doi: 10.20964/2018.12.66

International Journal of
ELECTROCHEMICAL
SCIENCE
www.electrochemsci.org

Corrosion inhibition performance of three antibacterial agents for mild steel in 1 M HCl solution at different temperature: experimental and theoretical studies

Xuanxuan Zhang [1], *Bochuan Tan* [2*]

[1] School of Economics and Business Administration, Chongqing University, China
[2] School of Chemistry and Chemical Engineering, Chongqing University, China
[*]E-mail: bochuantan@163.com

Received: 31 July 2018 / *Accepted:* 24 September 2018 / *Published:* 5 November 2018

The inhibiting properties of corrosion inhibitors of norfloxacin (NFA), ciprofloxacin (CFA), and ofloxacin (OFA) for steel in 1 M HCl solution had been studied, respectively. Their corrosion inhibiting property was performed in 1 mol/L hydrochloric acid by potentiodynamic polarization (PDP) and electrochemical spectroscopy (EIS) tests at different temperatures range. The order of their corrosion inhibition efficiency is as follows: CFA > NFA > OFA. Polarization data suggest that the corrosion inhibitors are predominantly mixed-type. The best fit for inhibitors adsorption is obey Langmuir isotherm model. The structure properties of corrosion inhibitors are correlated by means of a density-functional quantum-chemical approach. Moreover, the molecular dynamics calculation vividly simulates the adsorption behavior of CFA, NFA and OFA molecules on the surface of steel.

Keywords: Corrosion; Inhibition; Mild steel; Acid**;** Molecular dynamics

1. INTRODUCTION

Mild steel is widely used due to its low price and good mechanical properties [1-9]. Hydrochloric acid are applied for removal oxidation products on steel surface [10-12]. In order to inhibit Fe dissolution and reduce acid consumption in this process [13]. Therefore, corrosion workers have studied corrosion inhibitors to suppress the occurrence of this corrosion process.

However, the biology toxicity of organic and inorganic compounds, such as chromate and organic phosphate because they can destroy the ecological environment, and what's more, there is restrict of the complexity in produce, expensive cost and a small quantity of output of the above compounds. Therefore, large number of researchers have begun to develop highly effective and environmentally friendly corrosion inhibitors, which do not contain heavy metals and nutrition salts according to green chemistry principle and viewpoint, become more significant [14, 15].

In recent years, many corrosion researchers have studied the corrosion inhibitors of steel in hydrochloric acid solution. Tawfik [16] studied alginate surfactant derivatives as an eco-friendly corrosion inhibitor for carbon steel in the acidic environment. However, the corrosion inhibition effect is not very significant. Liu et al.[17] studied the modification of natural chitosan by β-cyclodextrin as a green inhibitor of carbon steel in an acidic solution. However, they did not study the effect of temperature on the corrosion inhibition performance of β-cyclodextrin modified natural chitosan. Yousefi et al.[18] studied imidazole-based ionic liquids as regulators of corrosion inhibition of SDS on low carbon steel in hydrochloric acid solution. The ionic liquids may cause certain harm to the environment. Xia et al. [19] studied Self-Assembly and Anticorrosive Property of N‑Alkyl-4-[2-(methoxycarbonyl)vinyl] pyridinium Bromides on X70 Steel in an Acid Medium. They also did not discuss the environmental impact of Alkyl-4-[2-(methoxycarbonyl)vinyl] pyridinium Bromides.

In this work, ciprofloxacin (CFA), norfloxacin (NFA) and ofloxacin (OFA) (shown in Figure 1) were tested. These three compounds can be applied as the component of usual medicine, which is antibiotic and stable. Therefore, they can be used in special situation for high environmental request, such as industry cycle water, foods manufactory, because there is no toxicity to the environment and operate personnel [20]. The corrosion inhibition behavior of CFA, NFA, and OFA was researched by experimental and theoretical studies. The quantum chemical method and molecular dynamics calculation were also performed to discussion about the relationship between inhibition ability and their structural properties of the inhibitors.

2. MATERIALS AND METHODS

2.1 Materials

CFA, NFA as well as OFA, their purity more than 99%, (Figure1) were from Aldrich Chemical Co.

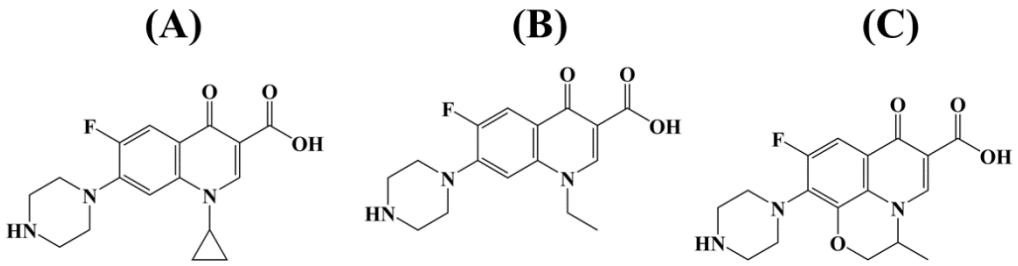

Figure 1. Three antibacterial agents structures of the inhibitors in this paper: (A) ciprofloxacin (1-cyclopropyl-6-fluoro-4-oxo-7-(1-piperazinyl)-1,4-dihydro-3-quinolinecarbox), (B) norfloxacin (1,4-dihydro-1-ethyl-6-fluoro-4-oxo-7-(1-piperazinyl)-3-quinolinecarboxylica), (C) ofloxacin ((+/-)-9-fluoro-2,3-dihydro-3-methyl-10-(4-methyl-1-piperazinyl)-7-oxo-7h-pyrido[1,2,3-de]-1,4-benzoxazine-6-carboxylic acid).

The corrosion solutions were made by dilution of Analytical Grade 37% HCl with double-

distilled water. The test solutions were prepared by adding 1 mol/L HCl of the researched compounds. The concentrations without deaerating varied from 3.16×10^{-5} to 3.16×10^{-3} mol/L. The 1 M hydrochloric acid as the blank solution does not contain any corrosion inhibitor. The specimens of steel having weight percent composition of 0.017 % C，0.78 % Si，0.85 % Mn，0.0047 % P，0.017 % S and the rest of Fe were used. The steel specimens of weight loss tests were cut into 2.9×1.6× 1.6 cm^3. And polished with sandpapers 220#, 400#, and 600#, respectively, cleaned in distilled water, degreased in acetone with an ultrasonic bath, dried and weighed. And then the surface (1.6 cm×1.6 cm) were sealed by water-resistant glue. The working electrode of 1 cm^2 executed in the electrochemical test, polished with sandpapers 400#, 600#, 800#, rinsed with ultrapure water, degreased ultrasonically in acetone.

2.2 Weight loss experiment

Mild steel specimens were soaked in the corrosion solutions for 4 hours at 293 K, 303 K, 313 K and 323 K in triplicate, respectively. After that, the mild steel samples were taken out, washed in ultrapure water and acetone, respectively. Finally, dried and weighed.

2.3 Electrochemical measurement

Instruments employing for potentiodynamic polarization and capacitance measurements were an IM6e impedance and electrochemical measurement system (ZAHNER, Germany). Electrochemical tests were carried out via the three-electrode cell. Mild steel as working electrode, platinum (1.5 ×1.5 cm^2) as counter-electrode, and a saturated calomel electrode (SCE) as reference electrode at 293,303,313 and 323 K in triplicate, respectively. The system immersed in 1M HCl for 30 minutes before starting experiment. The impedance experiments were executed in the frequency range of 100 kHz to 20 mHz with ac signals of 10mV amplitude. The values of charge transfer resistance (R_{ct}), solution resistances (R_s) and double layer capacitor (C_{dl}) were obtained by SIM program. The potentiodynamic data were obtained from–200 mV SCE to +300 mV SCE with respect to the corrosion potential with the scan rate of 0.5 mV/s.

2.4 Quantum chemical research and Molecular dynamics simulation

The quantum chemical calculations of the researched corrosion inhibitors were executed with Gaussion 03W in DFT level, via 3-21G basis set. The energy of the highest occupied molecular orbital (E_{HOMO}) and the lowest unoccupied molecular orbital (E_{LUMO}), the dipole moment (μ) and energy difference ΔE (E_{LUMO}- E_{HOMO}) were acquired. The HOMO and LUMO were mapped.

The interaction between three researched inhibitors and the mild steel surface was calculated in a 3D box, which size was 2.4× 2.6× 4.8 nm^3. In order to confine their position the 6 layers of steel atoms were fixed. Finally, NVT specification as the simulation condition, the simulation time was 1000 ps.

3. RESULTS AND DISCUSSION

3.1 Weight loss experiment

The inhibition efficiency (IE%) and corrosion rate (R) with the concentration and temperature are shown in Figs 2、3 [12,21]. The IE % and R from weight loss were calculated by:

$$IE\% = (W_0 - W) / W_0 \times 100\% \quad (1)$$

$$R = W/(S^* t) \quad (2)$$

where W_0 and W are uninhibited and inhibited weight losses, respectively. Figure 2 (A) shows that the corrosion rate decreases markedly, the mild steel weight loss decreases with increasing inhibitor concentration at 303 K, reaching their lowest values 0.52, 0.66, 1.22 g/(cm^{-2} • a) at 3.16×10^{-3} mol/L(as sequence of CFA、NFA、OFA, and the following as the above), respectively. Figure 2 (B) shows that the increasing temperature accelerates the corrosion of mild steel, and increases the mild steel weight loss, reaching their highest values 8.02, 8.34, 12.23 g/(cm^{-2}·a), respectively . It can be seen from Figure 2(B) that corrosion rate increases sharply when reaching to 323 K, especially that of the metal immersing the uninhibited solution. The inhibitors have begun to desorb in a large scale with inhibition efficiency in some degree, and the surface of metal can not been protected any more, which results in the weight loss of metal increases sharply.

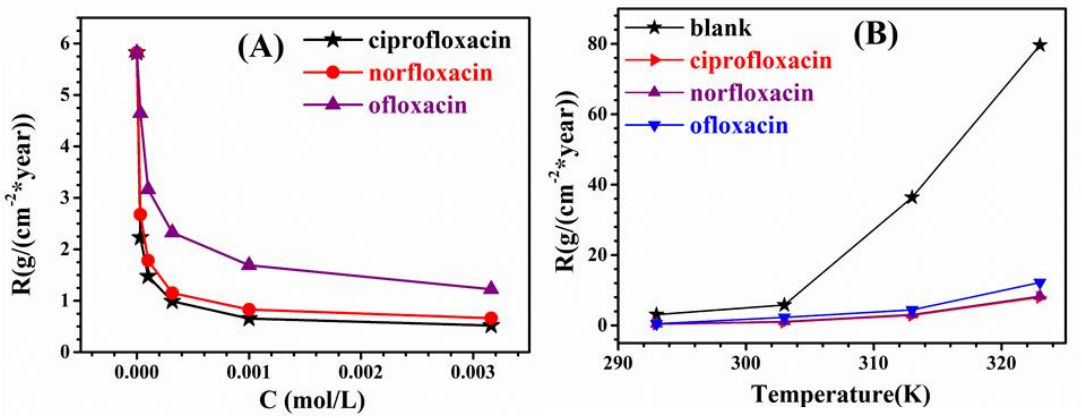

Figure 2. Corrosion rate for inhibitors on steel in 1 M HCl (A): at 303 K; (B): at 293,303,313,323 K with the concentration of 3.16×10^{-4} mol/L, respectively.

Figure 3 (A) shows that IE% increases markedly with the concentration of research compound increases at 303 K, reaching its highest value 91.95 %, 88.10 %, 79.50 % at 3.16×10^{-3} mol/L, respectively. Figure 3 (B) shows that the increasing temperature does not reduce the IE %, reaching its highest value 91.96%, 91.41%, 87.73 % at 313 K, respectively. However, IE% decreases at 323 K, which may be resulted from the surface desorption of inhibitors. All above results indicate that the compounds could act as the perfect acid inhibitors.

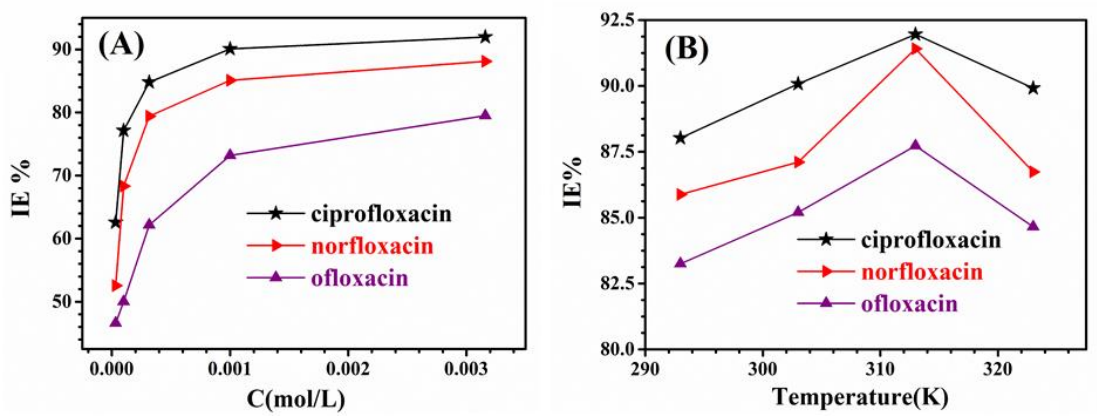

Figure 3. Inhibition efficiency for steel in 1 M HCl (A): at 303 K; (B): at 293,303,313,323 K with the concentration of 3.16×10^{-4} mol/L, respectively.

3.2 Electrochemical measurement

3.2.1 Electrochemical impendence spectroscopy

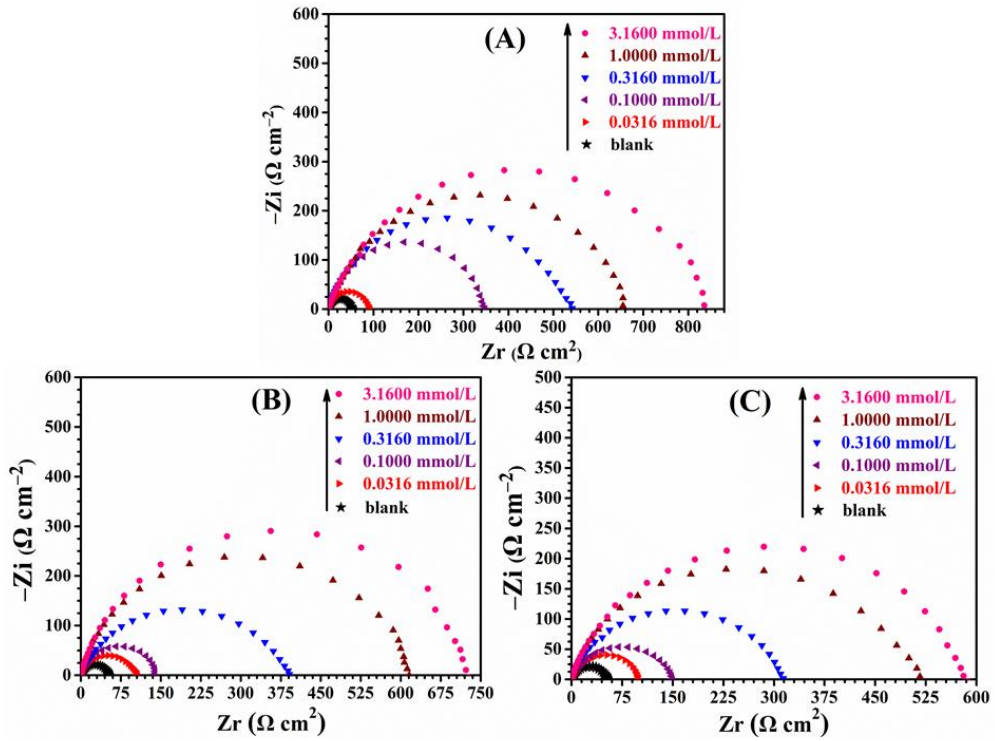

Figure 4. Nyquist plots for steel in 1 M HCl at 303 K. (A): CFA; (B): NFA; (C): OFA.

The Nyquist plots for mild steel at different concentrations inhibitors at 303 K are shown in Figure 4. The Figure shows that impedance spectra are similar in a single capacitive loop, which indicates that charge transfer controls corrosion process [23]. As the concentration of CFA, NFA, and OFA increases, the radius of the capacitive anti-arc increases significantly, and the imperfect

semicircles occur due to the inhomogeneity of the steel surface [24, 25]. These electrochemical system are typical corrosion systems of metal in acid correlated corrosion electrochemical parameters can be obtained by virtue of the equivalent circuit diagram (Figure 6). Where, R_s is the electrolyte resistance, R_{ct} is charge transfer resistance, C_{dl} are constant phase elements modeling the capacitance. Impedance parameters by SIM program for all compounds are given in Table 1. Inhibition efficiency (IE) calculated as following by Eq. (1) [11, 22, 26]:

$$IE\%=(R_{ct}-R'_{ct})/R_{ct}\times 100 \quad (3)$$

where R'_{ct} and R_{ct} are the values of charge transfer resistance with and without inhibitors, respectively. Figure 4 shows that the system changes in the presence inhibitors. At 3.16×10^{-5} mol/L and 1.0×10^{-4} mol/L, compounds do not inhibit evidently, R_{ct} increases and C_{dl} decrease slightly. While the inhibition effect increased markedly with increasing inhibitor concentration, R_{ct} increases reaching highest value 835 Ω/cm^2, 719 Ω/cm^2, 519 Ω/cm^2, respectively; C_{dl} decreases reaching lowest value 8 uF/cm^2, 18 uF/cm^2, 12 uF/cm^2, respectively; and inhibition efficiency increases reaching highest value 94.0%, 93.0%, 91.5% at 3.16×10^{-3} mol/L, respectively. It is well known that R_{ct} represents the corrosion rate of corrosion reaction and C_{dl} represents the inhibitors adsorption properties on metal surface. The values of C_{dl} decrease as the concentration of CFA, BFA, and OFA increases, due to the replacement of water molecules on the surface of the steel electrode by the corrosion inhibitor molecules [10, 13, 20]. It can be deduced from Figure 4 and Table 1 that the sequence of inhibition effect is as following: CFA > NFA> OFA. The corrosion resistance from CFA is strongest, the corrosion rate is lowest, and OFA is the worst than others.

Table 1 Impendence data of mild steel in 1 M HCl for researched inhibitors at 303 K.

	C (mmol/L)	R_s (Ω/cm^2)	C_{dl} (uF/cm^2)	R_{ct} (Ω/cm^2）	IE (%)
Blank	0	0.60	320	50	/
CFA	3.16×10^{-2}	0.51	94	88	43.2
	1.0×10^{-1}	0.57	29	340	85.2
	3.16×10^{-1}	0.75	17	550	90.0
	1	0.48	11	654	92.3
	3.16	0.52	8	835	94.0
NFA	3.16×10^{-2}	0.46	70	104	51.9
	1.0×10^{-1}	0.47	63	136	63.2
	3.16×10^{-1}	0.59	31	390	87.2
	1	0.92	27	594	91.5
	3.16	0.67	18	719	93.0
OFA	3.16×10^{-2}	0.46	79	96	47.9
	1.0×10^{-1}	0.54	47	145	64.8
	3.16×10^{-1}	0.65	22	315	84.1
	1.0×10^{-1}	0.68	15	511	90.2
	3.16×10^{-1}	0.66	12	591	91.5

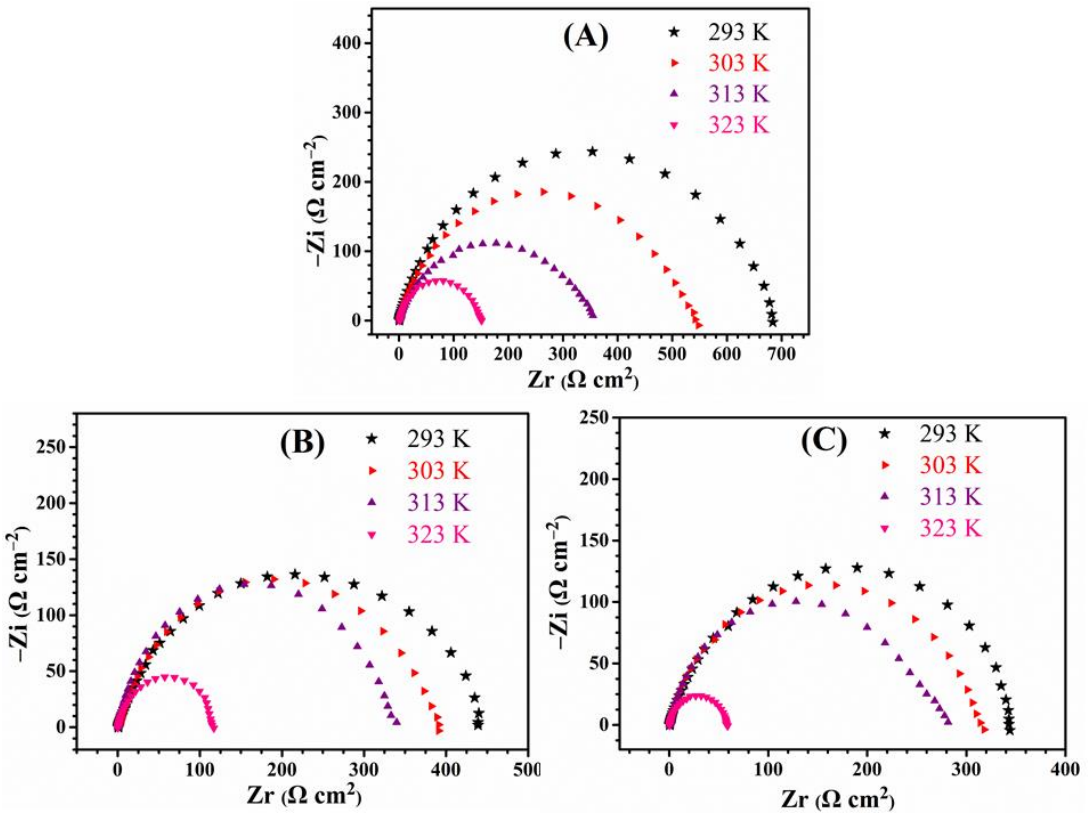

Figure 5. Nyquist plots for mild steel in 1 M hydrochloric acid for inhibitors at 3.16×10^{-4} mol/ L (A): CFA, (B): NFA, (C): OFA.

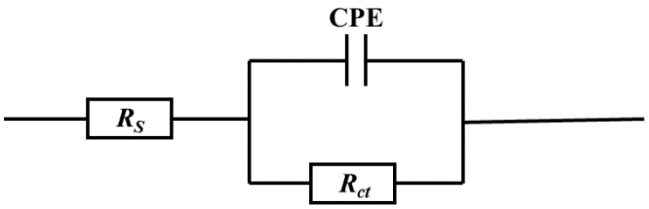

Figure 6. Best equivalent circuit diagram for fitting impedance spectrum data.

Nyquist plots for mild steel at 293, 303, 313, and 323 K of each inhibitor with 3.16×10^{-4} mol/L are shown in Figure 5, respectively. Figure 5 shows that impedance spectra are still a single capacitive loop with different temperatures. This electrochemical system can be interpreted by Figure 6. Impedance parameters by SIM program for all compounds are given in Table 2. Figure 5 shows that R_{ct} decreases and C_{dl} increases markedly at all concentrations. On the one hand, the R_{ct} decrease indicates that temperature increase results in the decreasing resistance sharply from the inhibitors adsorption film on the surface of metal; on the other hand, C_{dl} increase manifests that temperatures increase results in the increase of charge transfer sharply between the inhibitors adsorption film and the metal surface [13, 27]. Therefore, temperature increase goes against the inhibition effect. Figure 5 and Table 2 indicate that CFA still show good inhibition efficiency with different temperatures, however, OFA shows decreasing inhibition efficiency markedly with increasing temperature, which maybe result

from inhibitors vast desorption from the metal surface at high temperature (323K). Fig.7 validates visually the above phenomenon.

Table 2. Impendance data of mild steel at 1 M hydrochloric acid for inhibitors at 293K-323K

T (K)	Species	R_s (Ω/cm^2)	C_{dl} (uF/cm^2)	R_{ct} (Ω/cm^2)	IE (%)
293	Blank	0.49	260	65	/
	CFA	0.68	15	680	90.4
	NFA	0.79	16	436	85.1
	OFA	0.75	17	340	80.9
303	Blank	0.60	320	50	/
	CFA	0.75	17	550	90.9
	NFA	0.59	31	390	87.1
	OFA	0.65	22	315	80.9
313	Blank	0.99	470	34	/
	CFA	0.79	28	342	90.1
	NFA	0.65	48	335	89.8
	OFA	0.65	50	270	86.7
323	Blank	0.85	580	15	/
	CFA	0.82	34	153	83.6
	NFA	0.58	78	120	87.5
	OFA	0.57	60	58	74.1

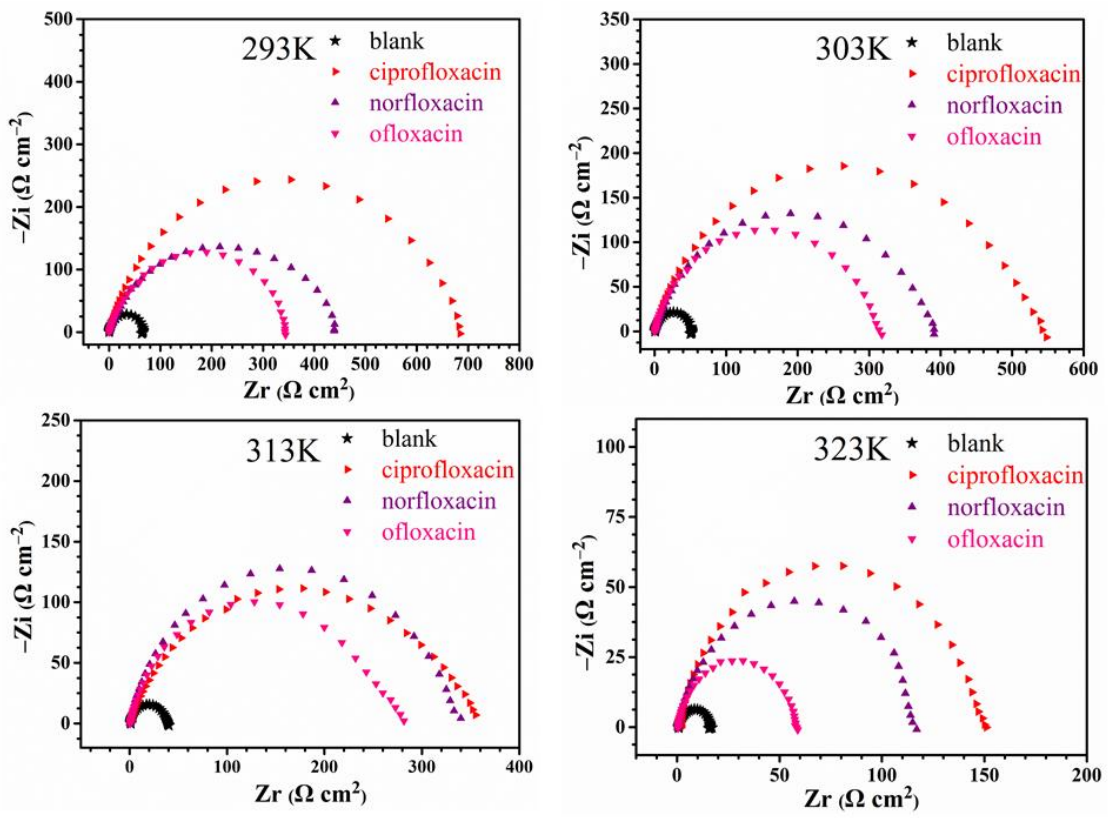

Figure 7. The Nyquist plots of mild steel in 1 M HCl for inhibitors at 3.16×10^{-4} mol/ L.

3.2.2 Potentiodynamic polarization curves

Figures 8–10 show dynamic potential polarization curves obtained with all tested compounds. Tables 3-4 show the electrochemical kinetic parameters. The corrosion inhibition efficiencies are calculated by the following formula [28-32]:

$$IE\% = (i_{0,corr} - i_{corr})/i_{corr} \quad (4)$$

where $i_{0,corr}$ and i_{corr} correspond to current densities without and with inhibitors, respectively. Figure 8 and Table 3 show that the inhibitor efficiency of all compounds augments with increasing researched inhibitor concentration at 303 K, reaching their highest values 94.6%, 92.5%, 89.7% at 3.16×10^{-3} mol/L, respectively.

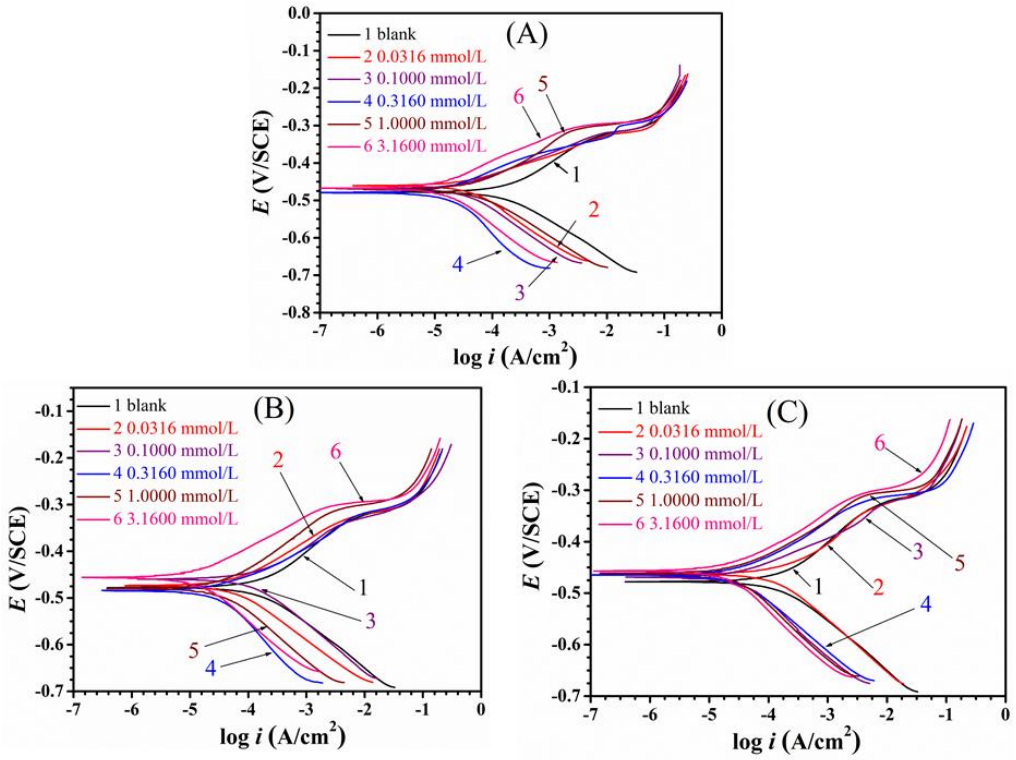

Figure 8. Potentiodynamic polarization curves of steel in 1 M hydrochloric acid with research inhibitors at 303 K. (A): CFA, (B): NFA, (C): OFA.

The corrosion potential E_{corr} shifts slightly not exceed 85 mV at all concentrations (Table 3), therefore, the researched compounds display mixed-type corrosion inhibition for steel in 1 M hydrochloric acid solution [33,34]. As the concentration of corrosion inhibitor increases, the corrosion current density decreases significantly, reaching their lowest value 13 uA/cm^2,18 uA/cm^2, 25 uA/cm^2, respectively. The polarization curves (Figure 8) show that CFA, NFA, and OFA have an effect on the cathodic and anodic slopes (β_c and β_a), β_c increased after the compounds added, and β_a became larger at all concentrations (Table.3) This hints change the mechanism of cathodic hydrogen evolution and anodic dissolution of Fe [35,36]. Figure 8 and Table 3 show that the i_{corr} for researched compounds in this experiment concentrations decreases in order of CFA > NFA > OFA, so, the inhibition result is still

CFA > NFA > OFA as well as that from EIS.

Figure 9 and Table 4 show that inhibitor efficiency of all compound decreases with increasing temperature, reaching their lowest values 80.9%, 81.5%, 72.6% at 3.16×10^{-4} mol/L, respectively. However, E_{corr} does not shift significantly with the increasing temperature, which indicates that the corrosion mechanism has not change. While, i_{corr} increases sharply with the increasing temperature, reaching the highest values 127 uA/cm^2, 123 uA/cm^2, 182 uA/cm^2 at 323 K, respectively, which indicates increasing temperature accelerates the corrosion rate. Increasing temperature deteriorates the corrosion of the steel surface, and metal ion dissolving from the metal surface increases markedly. At the same time, the inhibitors desorption from the surface accelerates because of the speed up of thermal motion, thus increasing temperature goes against the inhibition effect. Figure 9 and Figure 10 show that the inhibition result is still CFA > NFA > OFA with increasing temperature as well as the polarization curve at 303 K.

Table 3 Potentiodynamic polarization parameters at 303 K for steel in 1 M hydrochloric acid for researched corrosion inhibitors.

Species	C (mmol/L)	β_c (mV/dec)	β_a (mV/dec)	I (uA/cm^2)	E (mV)	IE (%)
Blank	0	80	38	242	–460	/
CFA	3.16×10^{-2}	90	49	80	–453	66.9
	1×10^{-1}	100	58	42	–456	83.4
	3.16×10^{-1}	98	69	31	–453	87.2
	1	103	76	22	–467	90.9
	3.16	118	83	13	–460	94.6
NFA	3.16×10^{-2}	80	54	92	–450	61.9
	1×10^{-1}	86	64	39	–461	83.9
	3.16×10^{-1}	110	68	33	–462	86.4
	1	105	80	31	–463	87.2
	3.16	108	82	18	–451	92.5
OFA	3.16×10^{-2}	95	47	70	–462	71.1
	1×10^{-1}	105	47	40	–495	83.5
	3.16×10^{-1}	94	66	30	–465	87.6
	1	106	64	28	–460	88.4
	3.16	105	68	25	–458	89.7

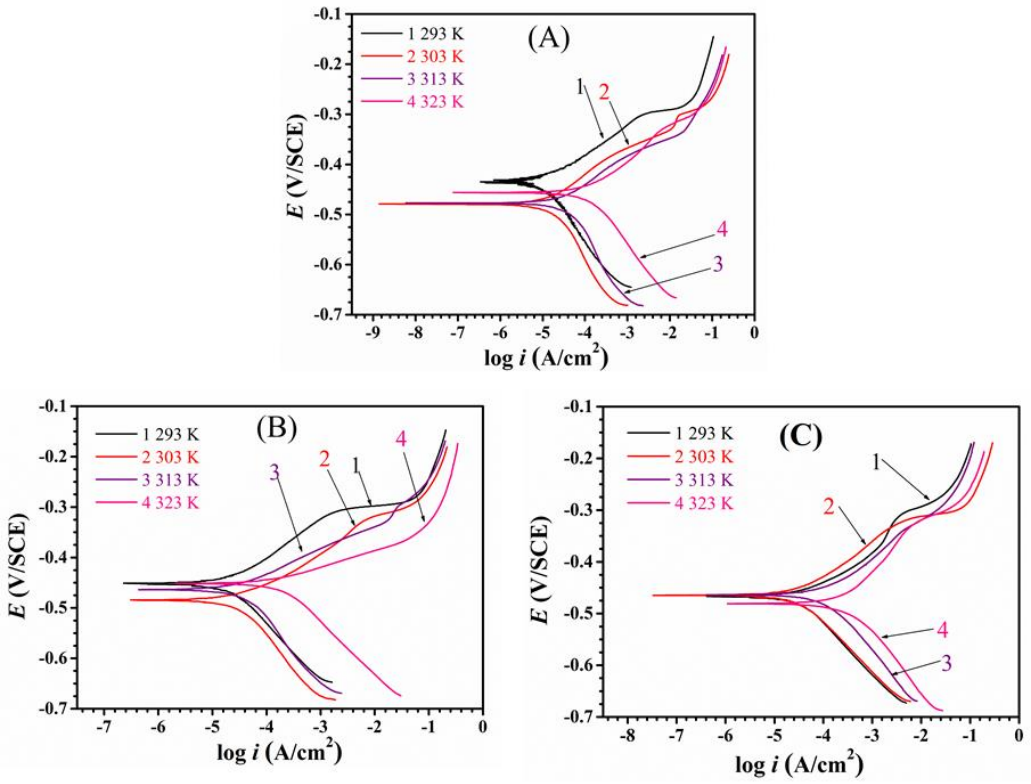

Figure 9. Potentiodynamic polarization curves of mild steel in 1 M hydrochloric acid with inhibitors at 3.16×10^{-4} mol/L. (A) CFA, (B) NFA, (C) OFA.

Table 4. Potentiodynamic polarization parameters for steel at 1 M HCl for inhibitors at 293 -323K.

T (K)	Species	β_c (mV/dec)	β_a (mV/dec)	I (uA/cm^2)	E (mV)	IE (%)
293	Blank	117	55	139	–473	/
	CFA	135	57	12	–433	91.4
	NFA	118	80	18	–454	87.0
	OFA	104	57	25	–470	82.0
303	Blank	80	38	242	–460	/
	CFA	98	69	31	–453	87.2
	NFA	110	68	33	–462	86.4
	OFA	94	66	30	–465	87.6
313	Blank	105	69	340	–464	/
	CFA	124	64	40	–457	88.2
	NFA	153	50	38	–453	88.9
	OFA	108	80	60	–469	82.4
323	Blank	97	78	665	–452	/
	CFA	116	65	127	–453	80.9
	NFA	111	66	123	–477	81.5
	OFA	113	73	182	–442	72.6

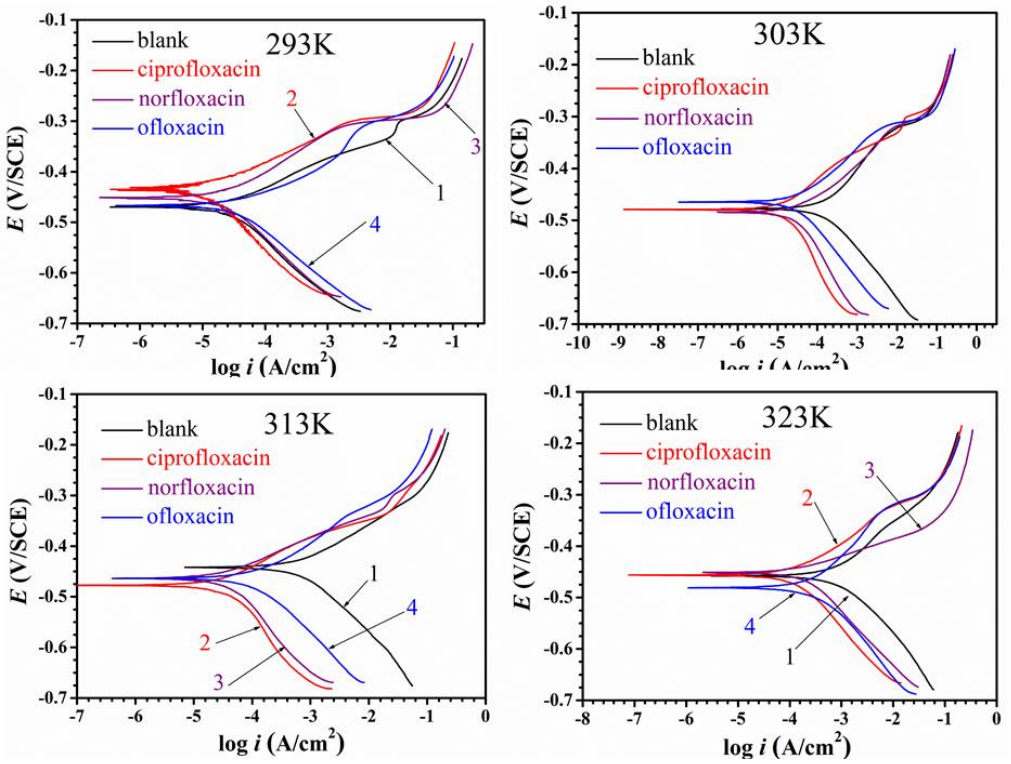

Figure 10. Potentiodynamic polarization curves for steel at 1 M HCl with inhibitors at 3.16×10^{-4} mol/L. (A) CFA, (B) NFA, (C) OFA.

3.3 Adsorption isotherm

The coverage degree (θ) is obtained by the following formula (5):

$$\theta = \frac{R_{ct}^{'} - R_{ct}}{R_{ct}^{'}} \times 100 \qquad (5)$$

Obviously, as the concentrations of CFA, NFA, and OFA increases, the values of coverage increase significantly. A variety of isothermal adsorption equations were used to fit the adsorption of CFA, NFA, and OFA molecules on the steel surface. The results show that Langmuir adsorption is most suitable. Its expression is shown in Equation 6 [37-44]. According to Equation 7, we can calculate the Gibbs free energy of the reaction.

$$\frac{C}{\theta} = C + \frac{1}{K} \qquad (6)$$

$$K = \frac{1}{55.5}\exp\left(\frac{\Delta G_{ad}^{0}}{RT}\right) \qquad (7)$$

where 55.5 is the molar concentration of H_2O molecule. Figure 11 presents the perfect fitting data with the correlation coefficient (R^2) 0.99999, 0.99969, 0.99968 of CFA, NFA and OFA, respectively. The equilibrium constants (K) are 4.21×10^6, 2.98×10^6, and 2.85×10^6 and the obtained values ΔG_{ads}^{0} are –48.54, –47.67 and –47.55 kJ/mol for CFA, NFA and OFA at 303 K, respectively. All compounds presents high K values at 303 K, manifesting that they are strong adsorption on the

surface of steel [1]. The negative values of ΔG_{ads}^{0} indicate that CFA, NFA and OFA are spontaneously adsorbed on the steel surface [17, 45, 46]. In addition, the absolute value of ΔG_{ads}^{0} exceeds 40 kJ/mol, indicating that CFA, NFA and OFA are mainly chemically adsorbed on the steel surface [39, 47, 48]. And it can be seen that ciprofloxacin adsorbs strongest on the metal surface from the values obtained.

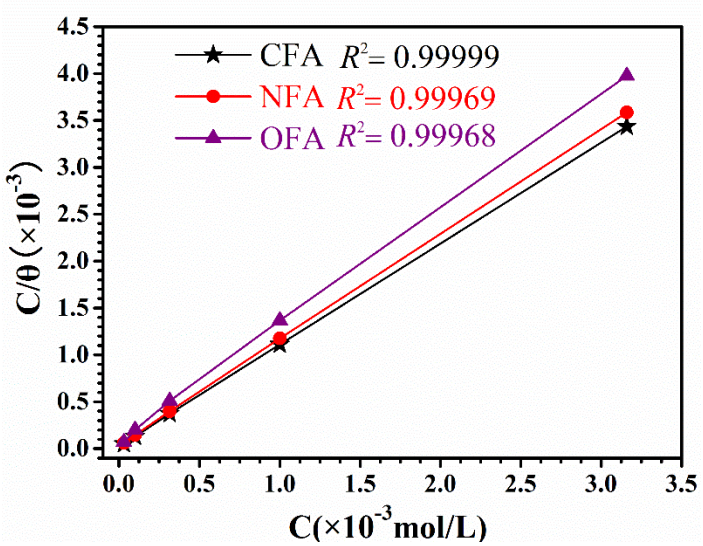

Figure 11. CFA, NFA, and OFA of Langmuir adsorption isotherm in 1 mol/L HCl at 303 K for steel.

3.4 Quantum chemical research

The CFA, NFA, and OFA optimized geometry are shown in Figure 12. The parallel structure of CFA, NFA, and OFA facilitates adsorption on metal surface. Some quantum chemical parameters are showed in Table 5. We know, The Fe contains 3d empty orbits, this unfilled 3d empty orbit can be bonded to the lone pair of corrosion inhibitor molecules. Figure 13 shows the electron cloud density distribution of CFA, NFA, and OFA. Only the energy highest/lowest ones of the two spin degeneracy orbital are taken into account here. For the HOMO, it can be found that cycle pyridine of all compounds have larger electric density and are more favour to bind with Fe 3d orbital. For the LUMO, cycle quinoline and O atoms of carboxyl of all compounds had larger electron density and could interact preferentially with Fe 4s orbital. It can be found that CFA has the largest electron orbital density whether E_{HOMO} or E_{LUMO}, which cause the highest inhibition efficiency [49]. As well known, E_{HOMO} was associated with ability of electron donating the molecule [10,13]. Table.5 indicts the relationship between HOMO energy and inhibition efficiency of the compounds, but LUMO energy does not give a linear relationship [50,51]. The lower ΔE cause higher inhibition efficiency, also which is proved that CFA with the lowest ΔE (Table.5) shows the best inhibition effect. High dipole (Table.5), especially that of CFA, also makes for the inhibitors physical adsorption to surface of Fe being in favor of the improvement ability of the inhibition [52,53]. We can be concluded that the CFA, NFA, and OFA, which had approximat planar structure could form firm and uniform adsorption layer on the mild steel surface. Both bindings strengthened chemical interaction from the evidence that large negatives

ΔG^0_{ads} values (–48.54, –47.67, and□–47.55 kJ/mol, respectively) were obtained.

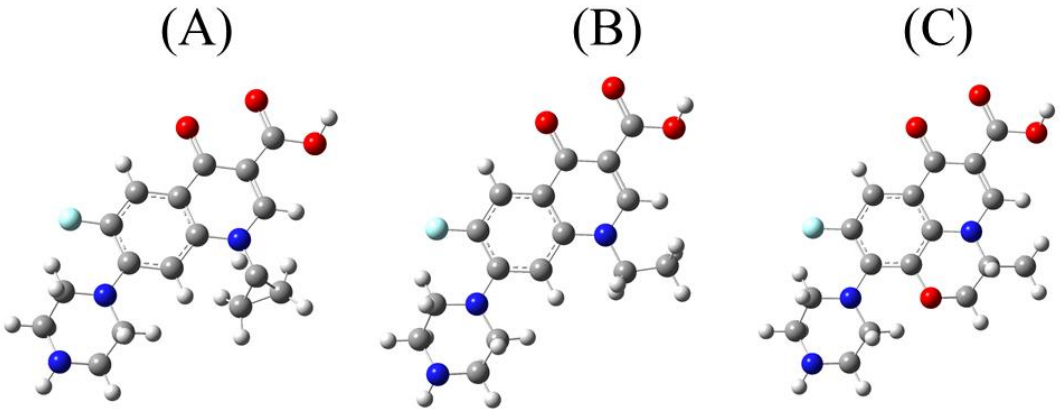

Figure 12. Optimized geometry for inhibitors: (A) CFA; (B) NFA; (C) OFA.

Table 5.The parameters of quantum chemical of all compounds.

Quantum parameters	E_{HOMO} (a.u)	E_{LUMO} (a.u)	$\Delta E_{(LOMO-HOMO)}$ (a.u)	μ (Debye)
CFA	□0.19227	□0.04153	0.15074	9.7654
NFA	□0.19901	□0.04071	0.15830	9.3929
OFA	□0.20491	□0.05063	0.15428	9.0235

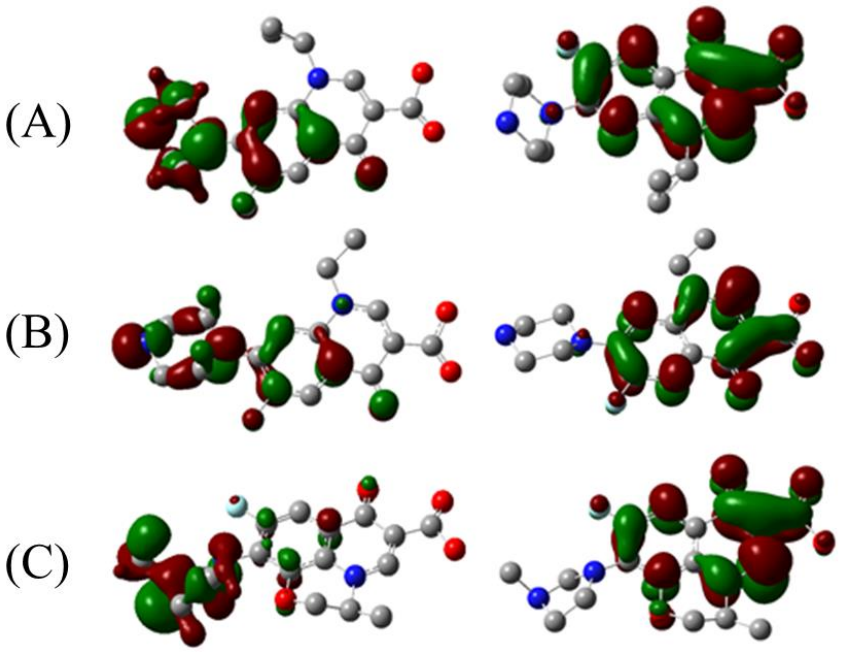

Figure 13. The electron cloud density map: (a) CFA (left: HOMO; right: LUMO), (b) NFA (left: HOMO; right: LUMO), (c) OFA (left: HOMO; right: LUMO).

3.5 Molecular dynamics simulation

Molecular dynamics simulation (MDS) studies have predictive and evaluation implications for

the interaction between CFA, NFA, and OFA molecules and metal matrices. In this work, MD simulation was executed to study their mechanism. As shown in Figure 14.

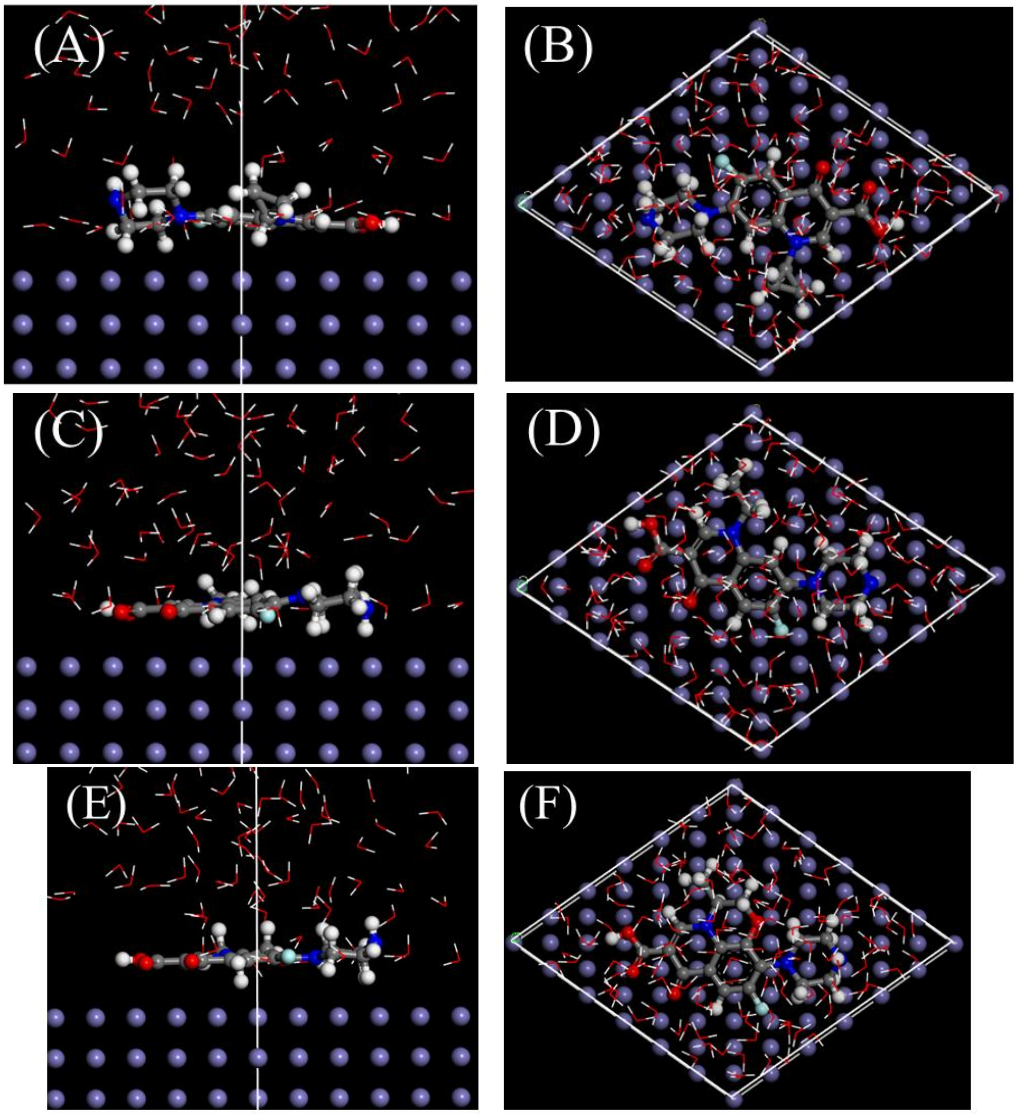

Figure 14. Equilibrium adsorption configurations of three corrosion inhibitor molecules on the Fe (110) surface: CFA side view (A) and top view (B), NFA side view (C) and top view (D), OFA side view (E) and top view (F).

The top and side views of stable equilibrium adsorption configurations of CFA, NFA, and OFA molecules on the Fe (110) surface. The CFA, NFA, and OFA molecules all adsorbed on the mild steel surface via the parallel way. Furthermore, the E_{interact} is defined with formula (8) as following [54-57]:

$$E_{interact} = E_{tot} - (E_{subs} + E_{inh}) \quad (8)$$

wherein E_{tot} is the total energy. E_{subs} is the energy of Fe (110) and H_2O. E_{inh} is the research inhibitor energy. $E_{binding}$ is defined with formula (9) as following [58, 59]:

$$E_{binding} = -E_{interact} \quad (10)$$

The $E_{binding}$ values of CFA, NFA and OFA are 889.4 kJ/mol, 819.2 kJ/mol and 753.8 kJ/mol,

respectively. Apparently, the order of binding energy of the three corrosion inhibitor molecules of CFA, NFA and OFA is consistent with the electrochemical experiment.

4. CONCLUSION

CFA, NFA and OFA are effective inhibitors for steel in 1 M HCl. With increasing temperature, the inhibition efficiency has not dropped down but 323 K. The inhibition ability increases in sequence of OFA< NFA< CFA at all temperatures.

Electrochemical impendence spectroscopy displays mainly a single capacitive loop ascribed to the covering of inhibitor adsorption film on the surface of steel. Potentiodynamic polarization (PDP) curves indicated CFA, NFA and OFA belongs mixed-type inhibitors.

The data of quantum chemical calculation indicates that inhibition efficiency increased with the decreasing CFA, NFA and OFA molecule's HOMO energy and ΔE. High dipole especially also makes for the physical adsorption of CFA, NFA and OFA molecules on surface of mild steel. Molecular dynamics simulations demonstrate that three inhibitor molecules are adsorbed on the surface of the steel via a parallel manner.

References

1. G. Khan, W.J. Basirun, S.N. Kazi, P. Ahmed, L. Magaji, S.M. Ahmed, G.M. Khan, M.A. Rehman, A. Badry, *J. Colloid Interf. Sci.,* 502 (2017) 134.
2. M. I. Awad, A.F. Saad, M.R. Shaaban, B.A.A. Jahdaly, O.A. Hazazi, *Int. J. Electrochem. Sci.,* (2017) 1657.
3. E.-S. M. Sherif, *Int. J. Electrochem. Sci.,* (2017) 1600.
4. H. Vashisht, I. Bahadur, S. Kumar, M.S. Goyal, G. Kaur, G. Singh, L. Katata-Seru, E.E. Ebenso, *J. Mol. Liq.,* 224 (2016) 19.
5. L. Yohai, M.B. Valcarce, M. Vázquez, *Electrochim. Acta,* 202 (2016) 316.
6. M.A. Deyab, *Electrochim. Acta,* 202 (2016) 262.
7. X. Zheng, M. Gong, C. Liu, *Int. J. Electrochem. Sci.,* (2017) 5553.
8. W. Zhao, H. Zhang, Y. Zou, *Int. J. Electrochem. Sci.,* (2017) 679.
9. S. Ullah, M.A. Bustam, A.M. Sharif, G. Gonfa, M. Ayoub, M. Raihan, *Int. J. Electrochem. Sci.,* (2017) 1642.
10. Y. Qiang, S. Zhang, B. Tan, S. Chen, *Corros. Sci.,* 133 (2018) 6.
11. P. Kannan, T.S. Rao, N. Rajendran, *J. Colloid Interf. Sci.,* 512 (2018) 618.
12. P. Han, C. Chen, W. Li, H. Yu, Y. Xu, L. Ma, Y. Zheng, *J.Colloid Interf. Sci.,* 516 (2018) 398.
13. B. Tan, S. Zhang, Y. Qiang, L. Feng, C. Liao, Y. Xu, S. Chen, *J. Mol. Liq.,* 248 (2017) 902.
14. A. Ehsani, M.G. Mahjani, M. Hosseini, R. Safari, R. Moshrefi, H. Mohammad Shiri, *J. Colloid Interf. Sci.,* 490 (2017) 444.
15. C. Verma, E.E. Ebenso, M.A. Quraishi, *J. Mol. Liq.,* 233 (2017) 403.
16. S. M. Tawfik, *RSC Advances,* 5 (2015) 104535.
17. Y. Liu, C. Zou, X. Yan, R. Xiao, T, Wang. M. Li, *Ind. Eng. Chem. Res.,* 54 (2015) 5664.
18. A. Yousefi, S. Javadian, N. Dalir, J. Kakemam, J. Akbari, *RSC Advances,* 5 (2015) 11697.
19. G. Xia, X. Jiang, L. Zhou, Y. Liao, *Ind. Eng. Chem. Res.,* 54 (2015) 1047.
20. B. Tan, S. Zhang, Y. Qiang, L. Guo, L. Feng, C. Liao, Y. Xu, S. Chen, *J. Colloid Interf. Sci.,* 526 (2018) 268.
21. C. Zhang, H. Duan, J. Zhao, *Corros. Sci.,* 112 (2016) 160.
22. L.L. Liao, S. Mo, H.Q. Luo, N.B. Li, *J. Colloid Interf. Sci.,* 520 (2018) 41.
23. Q. Ma, S. J. Qi, X. H. He, Y. M. Tang, G. Lu, *Corros. Sci.,* 129 (2017) 91.

24. A.K. Satapathy, G. Gunasekaran, S.C. Sahoo, K. Amit, P.V. Rodrigues, *Corros. Sci.,* 51 (2009) 2848
25. M. A. Amin, K.F. Khaled, Q. Mohsen, H.A. Arida, *Corros. Sci.,* 52 (2010) 1684.
26. Z. Zhang, N. Tian, W. Zhang, X. Huang, L. Ruan, L. Wu, *Corros. Sci.,* 111 (2016) 675.
27. K. S. Jacob, G. Parameswaran, *Corros. Sci.,* 52 (2010) 224.
28. M. A. Albuquerque, *Int. J. Electrochem. Sci.,* (2017) 852.
29. Z.Z. Tasic, M.M. Antonijevic, M.B. Petrovic Mihajlovic, M.B. Radovanovic, *J. Mol. Liq.,* 219 (2016) 463.
30. M.A. Azaroual, E.F. El Harrak, R. Touir, A. Rochdi, M.E. Touhami, *J. Mol. Liq.,* 220 (2016) 549.
31. J. Haque, V. Srivastava, C. Verma, M.A. Quraishi, *J. Mol. Liq.,* 225 (2017) 848.
32. L. Guo, G. Ye, I.B. Obot, X. Li, X. Shen, W. Shi, X. Zheng, *Int. J. Electrochem. Sci.,* (2017) 166.
33. L. L. Liao, S. Mo, J. L. Lei, H. Q. Luo, N. B. Li, *J. Colloid Interf. Sci.,* 474 (2016) 68.
34. G. Khan, W. J. Basirun, S. N. Kazi, P. Ahmed, L. Magaji, S. M. Ahmed, G. M. Khan, M. A. Rehman,A. B. Badry, *J. Colloid Interf. Sci.,* 502 (2017) 134.
35. A. Mishra, C. Verma, H. Lgaz, V. Srivastava, M.A. Quraishi, E. E. Ebenso, *J. Mol. Liq.,* 251 (2018) 317.
36. E. Alibakhshi, M. Ramezanzadeh, G. Bahlakeh, B. Ramezanzadeh, M. Mahdavian, M.Motamedi, *J. Mol. Liq.,* 255 (2018) 185.
37. M.B. Radovanović, M.M. Antonijević, *J. Adhesion Sci. Tech.,* 31 (2016) 369.
38. Y. Qiang, S. Zhang, L. Guo, S. Xu, L. Feng, I.B. Obot, S. Chen, *J. Clean. Prod.,* 152 (2017) 17.
39. M.M. Solomon, S.A. Umoren, *J. Colloid Interf. Sci.,* 462 (2016) 29.
40. X. Li, S. Deng, H. Fu, X. Xie, *Corros. Sci.,* 78 (2014) 29.
41. H. Lgaz, R. Salghi, S. Jodeh, B. Hammouti, *J. Mol. Liq.,* 225 (2017) 271.
42. K. Zhang, W. Yang, B. Xu, Y. Chen, X. Yin, Y. Liu, H. Zuo, *J. Colloid Interf. Sci.,* 517 (2018) 52.
43. J. Wysocka, S. Krakowiak, J. Ryl, *Electrochim. Acta,* 258 (2017) 1463.
44. S. Chen, A. Singh, Y. Wang, W. Liu, K. Deng, Y. Lin, *Int. J. Electrochem. Sci.,* (2017) 782.
45. S. Kumar, H. Vashisht, L. O. Olasunkanmi, I. Bahadur, H. Verma, M. Goyal, G. Singh, E. E. Ebenso, *Ind. Eng. Chem. Res.,*56 (2017) 441.
46. T. Gan, Y.J, Zhang, M.N. Yang, H.Y. Hu, Z.Q. Huang, Z.F. Feng, D. Chen, C.J. Chen, J. Liang. *Ind. Eng. Chem. Res.,*57 (2018) 10786.
47. P. Singh, E. E. Ebenso, L. O. Olasunkanmi, I. B. Obot, M.A. Quraishi, *Ind. Eng. Chem. Res.,*120 (2016) 3048.
48. X. Gao, S.T. Liu, H.F. Lu, F. Gao, H.Y. Ma, *Ind. Eng. Chem. Res.,*54 (2015) 1941.
49. L. Guo, S. Kaya, I.B. Obot, X. Zheng, Y. Qiang, *J. ColloidInterf. Sci.,* 506 (2017) 478.
50. Y. Qiang, S. Zhang, S. Xu, W. Li, *J. Colloid Interf. Sci.,* 472 (2016) 52.
51. A. S. Fouda, *Int. J. Electrochem. Sci.,* (2017) 347.
52. X. Zheng, S. Zhang, W. Li, M. Gong, L. Yin, *Corros. Sci.,* 95 (2015) 168.
53. X. Zheng, S. Zhang, W. Li, L. Yin, J. He, J. Wu, *Corros. Sci.,* 80 (2014) 383.
54. Y. Qiang, S. Zhang, L. Guo, X. Zheng, B. Xiang, S. Chen, *Corros. Sci.,* 119 (2017) 68.
55. I.B. Obot, Z.M. Gasem, *Corros. Sci.,* 83 (2014) 359.
56. L. Guo, S. Zhu, S. Zhang, Q. He, W. Li, *Corros. Sci.,* 87 (2014) 366.
57. Z. Wang, Y. Gong, C. Jing, H. Huang, H. Li, S. Zhang, F. Gao, *Corros. Sci.,* 113 (2016) 64.
58. Y. Qiang, S. Zhang, S. Yan, X. Zou, S. Chen, *Corros. Sci.,* 126 (2017) 295.
59. L. Ruan, Z. Zhang, X. Huang, Y. Lyu, Y. Wen, W. Shang, L. Wu, *Int. J. Electrochem. Sci.*, (2017) 103.